The Astrophysical Journal Letters, 842:L10 (5pp), 2017 June 20 https://doi.org/10.3847/2041-8213/aa775f

Probing Extreme-density Matter with Gravitational-wave Observations of Binary Neutron Star Merger Remnants

David Radice[1,2], Sebastiano Bernuzzi[3,4], Walter Del Pozzo[5], Luke F. Roberts[6], and Christian D. Ott[7]
[1] Institute for Advanced Study, 1 Einstein Drive, Princeton, NJ 08540, USA
[2] Department of Astrophysical Sciences, Princeton University, 4 Ivy Lane, Princeton, NJ 08544, USA
[3] Department of Mathematical, Physical and Computer Sciences, University of Parma, I-43124 Parma, Italy
[4] Istituto Nazionale di Fisica Nucleare, Sezione Milano Bicocca, gruppo collegato di Parma, I-43124 Parma, Italy
[5] Dipartimento di Fisica "Enrico Fermi," Università di Pisa, Pisa I-56127, Italy
[6] NSCL/FRIB and Department of Physics & Astronomy, Michigan State University, 640 S Shaw Lane, East Lansing, MI 48824, USA
[7] TAPIR, Walter Burke Institute for Theoretical Physics, California Institute of Technology, 1200 E. California Boulevard, Pasadena, CA 91125, USA
Received 2017 May 4; revised 2017 May 24; accepted 2017 June 2; published 2017 June 14

Abstract

We present a proof-of-concept study, based on numerical-relativity simulations, of how gravitational waves (GWs) from neutron star merger remnants can probe the nature of matter at extreme densities. Phase transitions and extra degrees of freedom can emerge at densities beyond those reached during the inspiral, and typically result in a softening of the equation of state (EOS). We show that such physical effects change the qualitative dynamics of the remnant evolution, but they are not identifiable as a signature in the GW frequency, with the exception of possible black hole formation effects. The EOS softening is, instead, encoded in the GW luminosity and phase and is in principle detectable up to distances of the order of several megaparsecs with advanced detectors and up to hundreds of megaparsecs with third-generation detectors. Probing extreme-density matter will require going beyond the current paradigm and developing a more holistic strategy for modeling and analyzing postmerger GW signals.

Key words: gravitational waves – stars: neutron

1. Introduction

Gravitational waves (GWs) from merging neutron stars (NSs) offer a unique way to probe the physics of matter at densities a few times that of nuclear saturation. The phase evolution of the GW signal in the past several orbits before contact is affected by the stars' response to the companion tidal field. Its measurement could provide a model-independent way to infer the Love number of the NSs and thus the NS radii with a precision of $\sim$1 km or better (Damour et al. 2012; Del Pozzo et al. 2013; Read et al. 2013; Bernuzzi et al. 2015b; Hinderer et al. 2016; Hotokezaka et al. 2016; Lackey et al. 2017). Given that the mass distribution of known binary NSs is sharply peaked around 1.35 $M_\odot$ (Lattimer 2012), the inspiral phase will not probe the properties of matter at the highest densities that can be reached in NSs, which can have masses up to at least $\sim$2 $M_\odot$ (Demorest et al. 2010; Antoniadis et al. 2013).

On the other hand, it is expected that the most common outcome of NS mergers is the formation of a compact remnant temporarily supported against gravitational collapse by (differential) rotation over timescales of several milliseconds to minutes after merger (Rosswog & Davies 2003; Shibata & Taniguchi 2006; Baiotti et al. 2008; Sekiguchi et al. 2011a; Palenzuela et al. 2015; Baiotti & Rezzolla 2016; Foucart et al. 2016). This remnant is an efficient emitter of GWs (Bernuzzi et al. 2016). Their spectrum is complex, and its most prominent feature is a broad peak at frequency $f_2 \sim$ 2–4 kHz (Stergioulas et al. 2011; Bauswein & Janka 2012; Takami et al. 2014; Bauswein & Stergioulas 2015; Dietrich et al. 2016; Rezzolla & Takami 2016).

For a fixed total binary mass, there is an empirical relation linking f_2 and $R_{1.6}$, the radius of an isolated non-rotating 1.6 $M_\odot$ NS (Bauswein & Janka 2012; Hotokezaka et al. 2013). It has also been argued that the behavior of the derivative of f_2 with respect to the total mass could be used to constrain the maximum NS mass (Bauswein et al. 2014). The existence of these relations suggests that f_2 can be used to infer the properties of matter at densities larger than those achieved in the inspiral. Bernuzzi et al. (2015a), however, showed the existence of a universal relation between f_2 and the binary tidal coupling constant κ_2^T (e.g., Bernuzzi et al. 2014), which is a quantity encoding the *inspiral* properties of the binaries. Similar universal relations have also been found for other characteristic frequencies of the signal (Rezzolla & Takami 2016).

Is it then possible to probe the equation of state (EOS) at the highest densities with GW observations? For example, could GW observations of an NS merger remnant identify phase transitions occurring at densities larger than those of the inspiral, but still be relevant for massive isolated NSs? In this work, we show that the answer to both questions is "yes." However, these measurements are not possible on solely on the basis of existing fits for f_2 frequency in the postmerger GW spectrum.

Instead, they will require more sophisticated waveform modeling and analysis.

2. Methods

As a case study, we consider the late inspiral and merger of NS binaries simulated in full general relativity. We adopt two temperature and composition-dependent EOSs for this work: the DD2 EOS (Hempel & Schaffner-Bielich 2010; Typel et al. 2010) and the BHB$\Lambda\phi$ EOS (Banik et al. 2014). Both use the same description of nuclear matter, but the BHB$\Lambda\phi$ EOS also includes $\Lambda-$hyperons, self-interacting via $\phi-$meson exchange. Both EOSs are consistent with theoretical and experimental constraints and with astronomical observations of massive NSs. The DD2 and BHB$\Lambda\phi$ EOS predict maximum NS masses of 2.42 $M_\odot$ and 2.11 $M_\odot$, and $R_{1.6} = 13.17$ km and

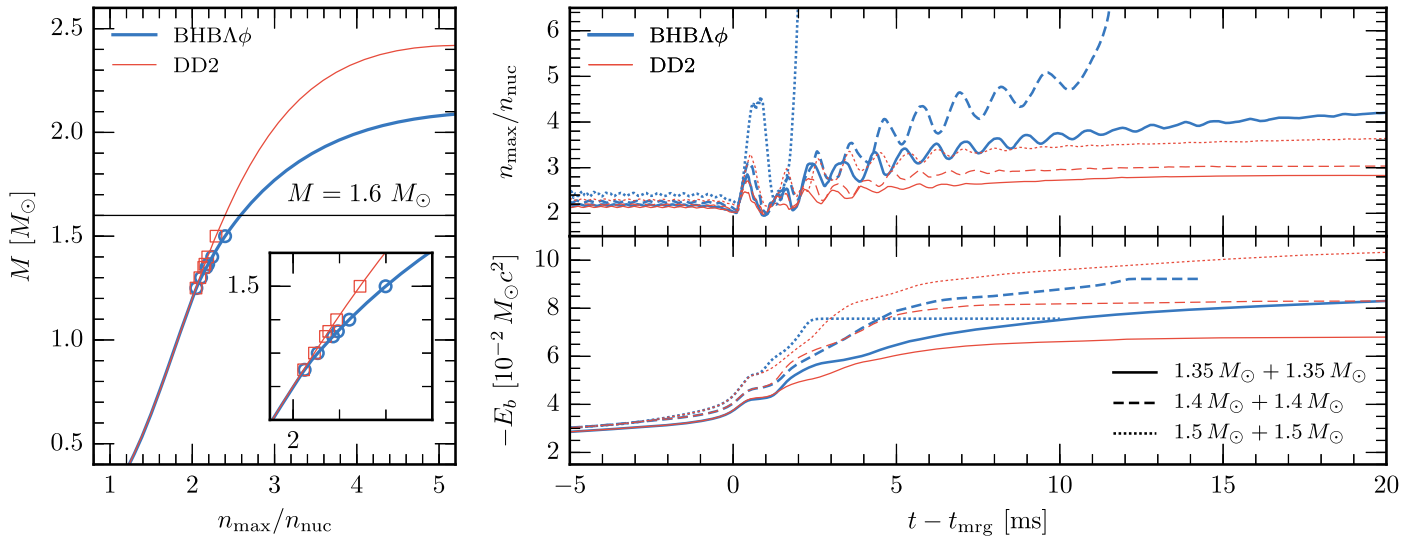

Figure 1. Left panel: mass–central density relations for spherical isolated NSs constructed with the BHBΛϕ and DD2 EOS. The symbols denote the individual components of the binaries we consider here. Right panel: maximum density (top) and binding energy (bottom) of the merger remnant relative to the binary at infinite separation for representative equal-mass binaries. The merger remnant becomes more compact and more bound with the BHBΛϕ EOS. The central densities reach values comparable to those in the most massive isolated NSs.

$R_{1.6} = 13.27$ km, respectively. The difference in $R_{1.6}$ is within the nominal error bars of the fits by Bauswein & Janka (2012) and Hotokezaka et al. (2013), so they both predict very similar f_2 GW frequency. We show the mass–central density curves for both EOSs in the left panel of Figure 1; see Figure 2 of Banik et al. (2014) for the mass–radius curves. Although our quantitative results are specific to these two EOSs, we expect our conclusions to generalize to all EOSs for which a high-density phase transition would be allowed by current constraints, in particular, the existence of $\simeq 2\,M_\odot$ NSs. The reason being that the main effects are a consequence of the EOS softening at densities larger than $\simeq 2.2\,n_{\rm nuc}$ and are not specific to the appearance of Λ-particles in the BHB Λϕ EOS. Here, we take $n_{\rm nuc} = 0.16\,{\rm fm}^{-3}$ (i.e., $\rho_{\rm nuc} \simeq 2.7 \times 10^{14}$ g cm^{-3}) as the nuclear saturation density.

We consider seven binaries with total (isolation) masses between 2.5 $M_\odot$ and 3 $M_\odot$, including two unequal-mass cases. We evolve each binary using both EOSs. For clarity, we discuss our qualitative results using three representative equal-mass binaries. Isolation NS masses and central densities of these binaries are highlighted in the left panel of Figure 1, and a full list is given in Figure 3. We simulate the last $\sim$ 3 orbits before merger and the evolution up to 21 ms after the time of merger $t_{\rm mrg}$, defined as the peak time of the GW strain amplitude.

For the simulations, we use the `WhiskyTHC` code (Radice et al. 2014), with the high-resolution setup described in Bernuzzi et al. (2016), improved with conservative mesh-refinement, not assuming rotational symmetry for equal-mass binaries, and extracting GWs at the larger distance of $\simeq$519 km. The linear resolution in the finest grid, covering both NSs during the inspiral and the merger remnant, is of $\sim$185 m. We verify the robustness of our results by repeating the 1.35 + 1.35 and 1.4 + 1.4 binary simulations (named after the isolation masses of the NSs) at 50% higher resolution. We also include neutrino cooling and lepton number changes following Radice et al. (2016). As in Radice et al. (2016), we use the finite-volume solver implemented in `WhiskyTHC` with high-order reconstruction of the primitive variables and an approximate Riemann solver.

Ours are the first fully general-relativistic merger simulations incorporating hyperons in a way consistent with all presently known EOS constraints.

3. Results

Comparing the evolutions with the two EOSs we find, unsurprisingly, negligible differences in the inspiral, because the EOSs agree at $n \lesssim 2.5\,n_{\rm nuc}$. Even for the most massive BHBΛϕ-1.5+1.5 binary, the hyperon (mass) fraction remains below 10% during the inspiral. This results in a small $\sim$5% increase of the central density during the inspiral; it has a very modest effect on the structure of the NSs and no measurable effect on the GW signal. This is in line with previous studies with hyperons using other EOSs (Sekiguchi et al. 2011b) or analytic approximations (Chatziioannou et al. 2015).

The merger process is characterized by a sudden compression of the stars followed by a rapid expansion; see the upper right panel of Figure 1 for the maximum density evolution of three representative binaries. At this time, the production of Λ-particles starts to become important for the dynamics. The formation of hyperons in the interface layer between the NSs during merger results in a catastrophic loss of pressure support, which leads to a more violent merger. In the most extreme case, BHBΛϕ-1.5+1.5, this results in a temporary increase of the maximum density from $\simeq 2\,n_{\rm nuc}$ to $\simeq 4.5\,n_{\rm nuc}$ immediately at merger, followed by a violent centrifugal bounce (Figure 1).

After merger, the BHBΛϕ remnants are characterized by a progressive increase of the hyperon fraction in their cores, which causes their rapid contraction, while the DD2 remnants remain more extended. The central densities reached in the BHBΛϕ binaries correspond to isolated NS masses of 1.8 $M_\odot$–2.0 $M_\odot$. This contraction is also reflected in an increase in magnitude of the binding energy of the binary (lower right panel of Figure 1), which is offset by correspondingly larger GW luminosities. This holds until black hole (BH) formation, at which point the GW emission shuts off. This occurs at 12.0 ms and 2.3 ms after merger for the most massive models

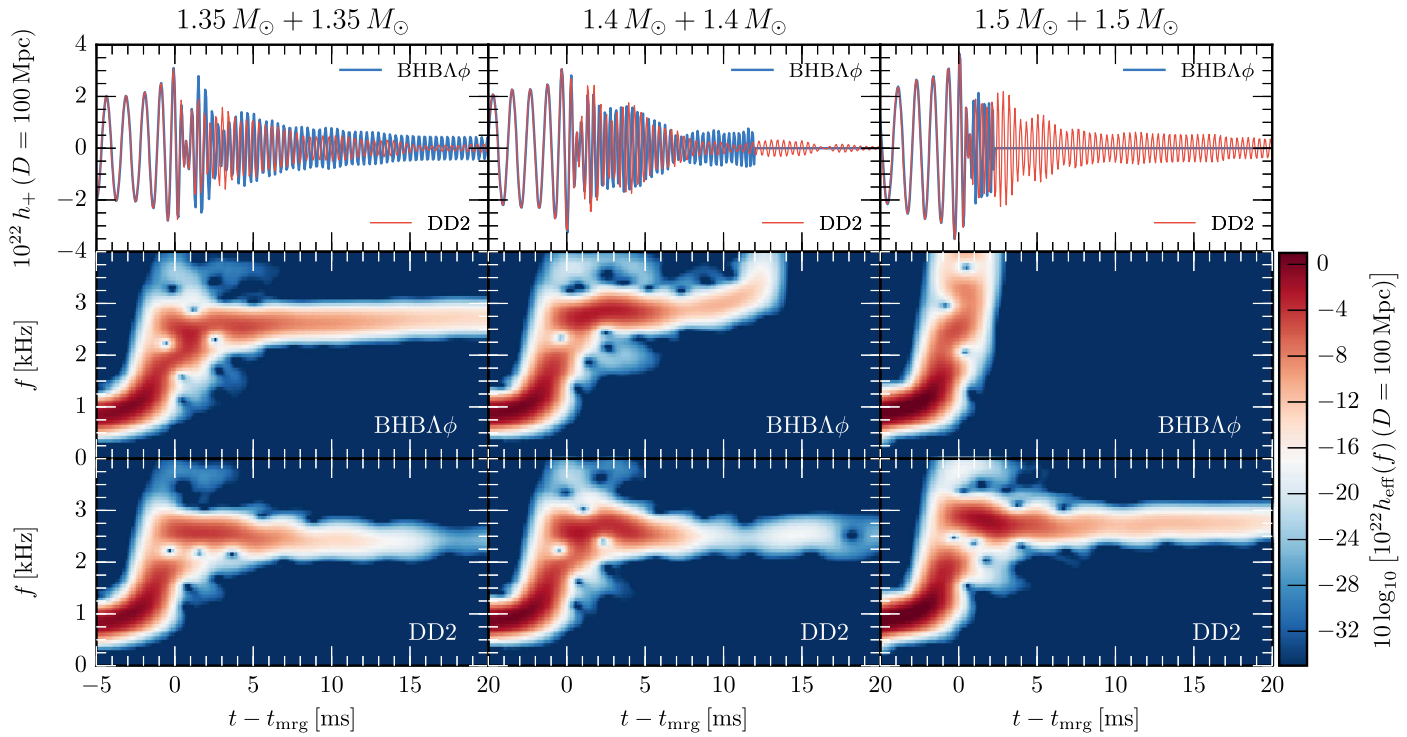

Figure 2. GW strain (top panel) and spectrograms (bottom panels) for three representative binaries assuming optimal orientation for the "+" polarization. The appearance of hyperons enhances the GW luminosity, but has only a modest impact on the GW peak frequency. The latter does not shows a significant evolution until shortly before BH formation.

with hyperons, BHBΛφ-1.4+1.4 and BHBΛφ-1.5+1.5, respectively. All other binaries result in remnants stable for the entire simulation time.

These qualitative features of the dynamics are reflected in the GW strain, which we show, for the same three binaries, in Figure 2. As anticipated, the waveforms start to be distinguishable only after merger, with the BHBΛφ binaries becoming significantly louder in GWs after merger and until BH formation (if it occurs). The spectral content of the signals is shown in the lower panels of Figure 2. Although the BHBΛφ signals show significant excess power compared with the DD2 ones, their peak frequencies are very similar. Indeed, the f_2 frequencies, which we extract from the spectrum of the entire postmerger signal, show differences smaller than the scatter of the relations found by Bauswein & Janka (2012), Hotokezaka et al. (2013), and Bernuzzi et al. (2014). For most binaries, these differences are below the nominal uncertainty of the Fourier transform ($\lesssim$50 Hz). Exceptions are the 1.4 + 1.4 and 1.5 + 1.5 binaries, where there are signatures of early BH formation. The former has $\Delta f_2 \simeq 250$ Hz, which is, however, still within the uncertainty of the relations of Bauswein & Janka (2012), Hotokezaka et al. (2013), and Bernuzzi et al. (2015a) for f_2. In the latter case, no postmerger frequency can be extracted for the BHBΛφ EOS, due to the prompt collapse.

We find evidence for small temporal drifts of the GW peak frequencies for both the DD2 and BHBΛφ binaries, which accelerate in the last few milliseconds prior to collapse. The peak-frequency drift for the binaries with hyperons is comparable in magnitude to that of the DD2 binaries and of other nucleonic EOS presented in the literature (Hotokezaka et al. 2013; Dietrich et al. 2016; Rezzolla & Takami 2016). Our results do not seem to support the suggestion by Sekiguchi et al. (2011b) that the production of hyperons might be encoded in the frequency evolution of the GW signal. They reinforce previous indications that the peak frequency of the GW signal, which has been the focus of all previous studies, is most sensitive to the relatively low-density, low-temperature part of the EOS relevant for the inspiral (Bernuzzi et al. 2015a).

It is important to remark that the BHBΛφ waveforms are not only louder than the DD2 waveform, they also have different amplitude modulation and phase evolution. These differences make the BHBΛφ and DD2 waveforms distinguishable. To quantify this observation, we window the waveforms to the interval $-1\,\mathrm{ms} \leqslant t - t_{\mathrm{mrg}} \leqslant 20\,\mathrm{ms}$ and compute optimal signal-to-noise ratios (S/Ns), i.e., assuming a perfect template, and fitting factors (FFs; Sathyaprakash & Schutz 2009; Del Pozzo et al. 2014) for Adv. LIGO, in its zero-detuning high-power configuration (Shoemaker 2010), and for the Einstein Telescope (ET), in its "D" configuration (Punturo et al. 2010; Hild et al. 2011). The FFs are computed by maximizing the match between the BHBΛφ and DD2 waveforms over time and phase shifts. In doing so, we implicitly assume that the maximum match parameters between the two waveforms are the same and that they coincide with their true values, which is reasonable since these parameters could be extracted from the inspiral signal. In our analysis, we also assume optimal orientation and sky position and limit ourselves to the single detector case. Additionally, we estimate the contribution of amplitude modulation by recomputing the FFs after having stretched the waveforms to remove any difference in the instantaneous phase evolution. We take the difference between the two FFs as a conservative measure of uncertainty.

Using FFs and S/Ns, we estimate the logarithm of the Bayes's factor against the presence of hyperons assuming DD2 to be nature's true EOS following the approach proposed by Vallisneri (2012) and Del Pozzo et al. (2014). For each binary,

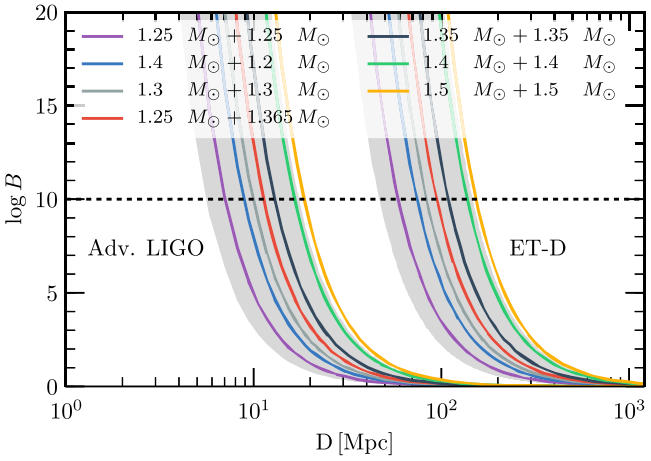

Figure 3. Distinguishability, as measured using the logarithm of the Bayes factor, between the DD2 and the BHB$\Lambda\phi$ EOS with Adv. LIGO and ET as a function of distance. Each line refers to a different binary. The gray shaded region denotes the uncertainty associated with the 1.35 + 1.35 binary, which is the most uncertain.

we estimate the Bayes's factor as a function of the distance. A similar calculation can be repeated, with quantitatively very similar results, assuming BHB$\Lambda\phi$ to be the true EOS and computing the detectability of hyperons. The results of the former analysis are shown in Figure 3. Large values of $\log B$ indicate that strong evidence against the presence of hyperons in the postmerger remnant would be available. Using Jeffrey's scale, $\log B \geqslant 6$ would constitute strong evidence and $\log B \geqslant 10$ would constitute decisive evidence (Kass & Raftery 1995). Correspondingly, in this idealized scenario with two EOSs to discern, Adv. LIGO could rule out one of the two possibilities with a single merger at a distance of up to $\sim$20 Mpc, depending on the total mass of the binary. This increases up to $\sim$200 Mpc with ET. We remark that these effective distances do not account for calibration uncertainty of the detectors and non-optimal orientation of the binaries, which would make these measurements even more challenging. At the same time, we do not consider the possibility of stacking multiple signals and/or data from multiple detectors, which could improve the prospects for detection.

4. Discussion

Our results show that the behavior of matter in the high-density postmerger stage is directly imprinted on the amplitude and phase of the GW signal. The postmerger GW peak frequency is, instead, mainly sensitive to matter properties at NS densities during inspiral. We have demonstrated that GW observations of NS merger remnants can be used to probe the EOS of nuclear matter at extreme densities.

Here, we have only considered the possible presence of interacting Λ-hyperons. In addition to Λ-hyperons, kaon or pion condensates (Pons et al. 2000), transitions to quark matter (Steiner et al. 2000), or the presence of other hyperons at high densities are all possible. Generally, phase transitions and extra degrees of freedom soften the EOS and increase the binding energy of remnants with fixed baryon number, similar to the BHB$\Lambda\phi$ model considered here. Therefore, we expect the presence of other exotic phases of matter to have impacts qualitatively similar to that of Λ-hyperons on the GW signal.

Our findings do not invalidate previously proposed approaches to the postmerger GW data analysis (e.g., Clark et al. 2014, 2016). We also do not exclude the possibility that constraints on the high-density EOS could be extracted from a more careful analysis of the GW peak frequency, going beyond existing phenomenological fits, for example, with the method suggested by Bauswein et al. (2014). However, on the basis of our results, we advocate a more ambitious approach based on a Bayesian analysis of GW data using full waveform templates, with amplitude and phase information, to extract the most likely values of parameters describing the high-density EOS.

The kind of model-dependent inference we are proposing, which we have shown to be able to probe the EOS at the highest densities, will require the availability of large banks of waveform templates. Possible avenues to follow are either the construction of reduced order models (Field et al. 2014; Pürrer 2014) or the use of a Gaussian process regression strategy (Gair & Moore 2015; Moore et al. 2016). Either requires large databases of numerical waveforms covering the binary parameter space for a variety of EOSs.

To be able to distinguish physical effects resulting in postmerger waveform mismatch $M = 1 - \mathrm{FF}$, it will be necessary to develop template waveforms with a mismatch to the real signal $M_{\mathrm{NR}} \ll M$. This accuracy requirement is stringent for low-mass binaries, for which the mismatches due to the appearance of hyperons are relatively small. Nevertheless, they are within reach. For example, for the 1.4 + 1.4 binary, our high-resolution and standard-resolution data already have a mismatch a factor $\sim$2 smaller than that due to hyperons. On the other hand, systematic uncertainties due to missing physics still need to be addressed. This will be the aim of our future work.

We thank S. Hild for the ET-D noise curve data and the anonymous referee for useful comments, and we acknowledge useful discussions with A. Burrows, T. Dietrich, S. Marka, L. Rezzolla, B. S. Sathyaprakash, and K. Takami. D.R. gratefully acknowledges support from the Schmidt Fellowship, the Sherman Fairchild Foundation and the Max-Planck/Princeton Center (MPPC) for Plasma Physics (NSF PHY-1523261). C.D.O. was partially supported by NSF awards CAREER PHY-1151197, PHY-1404569, and TCAN AST-1333520, and by the Sherman Fairchild Foundation. The simulations were performed on NSF XSEDE (TG-PHY160025), and on NSF/NCSA Blue Waters (NSF PRAC ACI-1440083).

References

Antoniadis, J., Freire, P. C. C., Wex, N., et al. 2013, Sci, 340, 6131
Baiotti, L., Giacomazzo, B., & Rezzolla, L. 2008, PhRvD, 78, 084033
Baiotti, L., & Rezzolla, L. 2016, arXiv:1607.03540
Banik, S., Hempel, M., & Bandyopadhyay, D. 2014, ApJS, 214, 22
Bauswein, A., & Janka, H. T. 2012, PhRvL, 108, 011101
Bauswein, A., & Stergioulas, N. 2015, PhRvD, 91, 124056
Bauswein, A., Stergioulas, N., & Janka, H. T. 2014, PhRvD, 90, 023002
Bernuzzi, S., Dietrich, T., & Nagar, A. 2015a, PhRvL, 115, 091101
Bernuzzi, S., Nagar, A., Balmelli, S., Dietrich, T., & Ujevic, M. 2014, PhRvL, 112, 201101
Bernuzzi, S., Nagar, A., Dietrich, T., & Damour, T. 2015b, PhRvL, 114, 161103
Bernuzzi, S., Radice, D., Ott, C. D., et al. 2016, PhRvD, 94, 024023
Chatziioannou, K., Yagi, K., Klein, A., Cornish, N., & Yunes, N. 2015, PhRvD, 92, 104008
Clark, J., Bauswein, A., Cadonati, L., et al. 2014, PhRvD, 90, 062004
Clark, J. A., Bauswein, A., Stergioulas, N., & Shoemaker, D. 2016, CQGra, 33, 085003
Damour, T., Nagar, A., & Villain, L. 2012, PhRvD, 85, 123007

Del Pozzo, W., Grover, K., Mandel, I., & Vecchio, A. 2014, CQGra, 31, 205006
Del Pozzo, W., Li, T. G. F., Agathos, M., Van Den Broeck, C., & Vitale, S. 2013, PhRvL, 111, 071101
Demorest, P., Pennucci, T., Ransom, S., Roberts, M., & Hessels, J. 2010, Natur, 467, 1081
Dietrich, T., Ujevic, M., Tichy, W., Bernuzzi, S., & Bruegmann, B. 2016, arXiv:1607.06636
Field, S. E., Galley, C. R., Hesthaven, J. S., Kaye, J., & Tiglio, M. 2014, PhRvX, 4, 031006
Foucart, F., Haas, R., Duez, M. D., et al. 2016, PhRvD, 93, 044019
Gair, J. R., & Moore, C. J. 2015, PhRvD, 91, 124062
Hempel, M., & Schaffner-Bielich, J. 2010, NuPhA, A837, 210
Hild, S., Abernathy, M., Acernese, F., et al. 2011, CQGra, 28, 094013
Hinderer, T., Taracchini, A., Foucart, F., et al. 2016, PhRvL, 116, 181101
Hotokezaka, K., Kiuchi, K., Kyutoku, K., et al. 2013, PhRvD, 88, 044026
Hotokezaka, K., Kyutoku, K., Sekiguchi, Y.-i., & Shibata, M. 2016, PhRvD, 93, 064082
Kass, R. E., & Raftery, A. E. 1995, J. Am. Stat. Assoc., 90, 773
Lackey, B. D., Bernuzzi, S., Galley, C. R., Meidam, J., & Van Den Broeck, C. 2017, PhRvD, 95, 104036
Lattimer, J. M. 2012, ARNPS, 62, 485
Moore, C. J., Berry, C. P. L., Chua, A. J. K., & Gair, J. R. 2016, PhRvD, 93, 064001
Palenzuela, C., Liebling, S. L., Neilsen, D., et al. 2015, PhRvD, 92, 044045
Pons, J. A., Reddy, S., Ellis, P. J., Prakash, M., & Lattimer, J. M. 2000, PhRvC, 62, 035803
Punturo, M., Abernathy, M., Acernese, F., et al. 2010, CQGra, 27, 084007
Pürrer, M. 2014, CQGra, 31, 195010
Radice, D., Galeazzi, F., Lippuner, J., et al. 2016, MNRAS, 460, 3255
Radice, D., Rezzolla, L., & Galeazzi, F. 2014, CQGra, 31, 075012
Read, J. S., Baiotti, L., Creighton, J. D. E., et al. 2013, PhRvD, 88, 044042
Rezzolla, L., & Takami, K. 2016, PhRvD, 93, 124051
Rosswog, S., & Davies, M. B. 2003, MNRAS, 345, 1077
Sathyaprakash, B. S., & Schutz, B. F. 2009, LRR, 12, 2
Sekiguchi, Y., Kiuchi, K., Kyutoku, K., & Shibata, M. 2011a, PhRvL, 107, 051102
Sekiguchi, Y., Kiuchi, K., Kyutoku, K., & Shibata, M. 2011b, PhRvL, 107, 211101
Shibata, M., & Taniguchi, K. 2006, PhRvD, 73, 064027
Shoemaker, D. 2010, Advanced LIGO Anticipated Sensitivity Curves, Tech. Rep. LIGO-T0900288-v3, LIGO Scientific Collaboration, https://dcc.ligo.org/cgi-bin/DocDB/ShowDocument?docid=t0900288
Steiner, A., Prakash, M., & Lattimer, J. M. 2000, PhLB, 486, 239
Stergioulas, N., Bauswein, A., Zagkouris, K., & Janka, H.-T. 2011, MNRAS, 418, 427
Takami, K., Rezzolla, L., & Baiotti, L. 2014, PhRvL, 113, 091104
Typel, S., Ropke, G., Klahn, T., Blaschke, D., & Wolter, H. H. 2010, PhRvC, 81, 015803
Vallisneri, M. 2012, PhRvD, 86, 082001